Effect Of Ionic Liquid On Semi–crystalline Poly(vinylidene fluoride–co–hexafluoropropylene) Solid Copolymer Electrolytes

Chiam–Wen Liew, Y. S. Ong, J. Y. Lim, C. S. Lim, K. H. Teoh, S. Ramesh[*]

Centre for Ionics University of Malaya, Department of Physics, Faculty of Science, University of Malaya, 50603 Kuala Lumpur, Malaysia
[*]E-mail: rameshtsubra@gmail.com

Solid copolymer electrolytes based on poly(vinylidene fluoride–co–hexafluoropropylene) (PVdF–HFP) as the host polymer, containing lithium perchlorate salt (LiClO$_4$) and 1–butyl–3–methylimidazolium chloride ionic liquid (BmImCl) had been prepared through solution casting method. The highest ionic conductivity of $(1.49\pm0.02)\times10^{-3}$ Scm^{-1} was achieved by doping 80 wt% of BmImCl at room temperature. These copolymer electrolytes followed Arrhenius rules as proven in temperature–dependence ionic conductivity study. X–ray diffraction (XRD) revealed lower crystalline portion of the polymer electrolytes. This has been further proven in differential scanning calorimetry (DSC) by determining the degree of crystallinity of copolymer electrolytes. Upon addition of 40 wt% of BmImCl, the glass transition, melting and crystallization temperatures are significantly reduced as visualized in DSC thermograms. However, both of melting and crystallization peaks are absent by adding more 40 wt% of BmImCl. Thermogravimetric analysis (TGA) demonstrated that the thermal stability of solid copolymer electrolytes was reduced upon addition of BmImCl. However, the stability of this ionic liquid–based solid copolymer electrolyte was up to 232 °C as proven in TGA curve.

Keywords: Ionic conductivity; transference number; XRD; DSC; Crystallinity

1. INTRODUCTION

A large number of researches had been done on polymer electrolyte due to its wider range of potential application such as lithium rechargeable batteries, electrochromic windows (ECWs), fuel cells, solar cells, supercapacitors, thermoelectric generators, analog memory devices and chemical sensors [1–3]. Nevertheless, the main application of polymer electrolytes is the lithium polymer battery. This high power density battery is essential for electrical and electrochemical devices, such as laptop, mobile phone, hybrid electrical vehicle (EV) and traction power source for electricity. Solid

polymer electrolytes are promising candidates to replace liquid electrolytes due to their inherent properties, such as less reactive to sealant and electrode, ease handling and high flexibility in geometry properties for the various applications. They get rid of the problems of corrosive solvent leakage and harmful gas compared to liquid electrolytes. For battery application, they manifest more advantages than conventional liquid electrolytes for example suppression of dendrite growth and great endurance in varying electrode volume during cycling. They are also much safer as solid polymer electrolytes do not build up the internal pressure which may causes the explosion during charge and discharge processes [4].

Plasticized–gel polymer electrolytes had received a lot attention recently due to relatively high ionic conductivity but they have some drawbacks such as low mechanical strength and less compatible with lithium metal anode [5]. Therefore, the attempt of using ionic liquids was applied to replace plasticizers. Ionic liquids are recognized as room temperature molten salts. They are commonly known as "green and designer" materials for chemical reactions. Low vapor pressure of ionic liquids makes them ideal replacement for volatile and conventional organic solvents in battery application. The ionic liquids were tailored to develop high ionic conductive polymer electrolytes [6]. Simple structural modifications onto the cations or anions have been made in order to design an optimized lithium ion polymer electrolyte [7].

Poly(vinylidene fluoride–co–hexafluoropropylene) (PVdF–HFP), lithium perchlorate ($LiClO_4$) and 1–butyl–3–methylimidazolium chloride (BmImCl) were used as host polymer , salt and ionic liquid, respectively in this present work. Poly(vinylidene fluoride–co–hexafluoropropylene) (PVdF–HFP) is a semi–crystalline polymer which composed of crystalline VdF unit and amorphous HFP units [8]. It is a talented candidate as matrix material for solid polymer electrolytes due to its attractive properties. These excellent characteristics are high solubility in various organic solvent, lower crystallinity, lower glass transition and melting temperatures, and high anodic stability due to strong electron withdrawing functional group [9–10]. In addition, it is an ideal material due to its high chemically resistance and relatively high dielectric constant ($\varepsilon=9.4–10.6$) and superior mechanical integrity as well as good electrochemical stability [11–12]. Since copolymerization is one of the effective approaches to enhance the ionic conductivity, thus this copolymer can also improve the ionic conductivity. Lithium perchlorate ($LiClO_4$) was chosen due to its larger size of anion. The larger anion could promote the lithium dissociation and result more charge carriers for transportation [13]. Lithium perchlorate has the merits of being a doping salt due to its satisfactory solubility, ease to handle, cost effective, high conductivity and enhanced anodic stability (up to 5.1V) as well. Comparing to other salts, it is more stable to ambient moisture and relatively less hygroscopic [14]. 1–butyl–3–methylimidazolium cation ($BmIm^+$) is a common and appealing cation because of its favorable properties and ease to gather abundant and useful information [15]. New proton conducting PVdF–HFP copolymer membranes consisting of 2,3–dimethyl–1–octylimidazolium trifluromethanesulfonylimide (DMOImTFSI) had been synthesized by Sekhon and co–workers. The maximum ionic conductivity of 2.74 m Scm^{-1} was achieved at 130 °C, along with good mechanical stability [16].

2. EXPERIMENTAL

2.1. Materials

Poly(vinylidene fluoride–co–hexafluoropropylene) (PVdF–HFP) with average molecular weight of 400000 gmol^{-1}, was obtained from Sigma–Aldrich. Lithium perchlorate (LiClO$_4$) was purchased from Aldrich, while 1–butyl–3–methylimidazolium chloride (BmImCl) was purchased from Acros organics. Reagent grade acetone was obtained from J.T. Baker.

2.2. Preparation of thin films

Table 1. Composition and designation of PVdF–HFP/LiClO$_4$/BmImCl polymer electrolyte thin films.

Designation	Weight ratio of materials (PVdF–HFP:LiClO$_4$:BmImCl)
IL0	70 : 30: 0
IL20	56 : 24 : 20
IL40	42 : 18 : 40
IL60	28 : 12 : 60
IL80	14 : 6 : 80

Ionic liquid–based polymer electrolytes were prepared using solution casting method. Table 1 depicts the composition of polymer electrolytes and their designations. PVdF–HFP, LiClO$_4$ and BmImCl were dissolved in acetone and stirred overnight at ambient temperature. The solutions were thus cast on Petri dish and allowed to evaporate slowly in ambient environment. A free standing polymer film was eventually produced.

2.3. Characterization

All the samples were subjected to ac–impedance spectroscopy, transference number measurement with DC polarization, x–ray diffraction (XRD) , differential scanning calorimetry (DSC) and thermogravimetric analysis (TGA) for characterization.

2.3.1. Ionic conductivity studies

Freshly prepared samples were subjected to HIOKI 3532–50 LCR HiTESTER in a frequency range of 50 Hz–5 MHz for conductivity measurements. A fixed voltage of 0.010V was applied across the solid copolymer electrolytes. The conductivity measurement was performed in the configuration of stainless steel (SS)/copolymer electrolytes/ stainless steel (SS). The ionic conductivity of polymer electrolytes was determined as follow:

$$\sigma = \frac{l}{AR_b} = \frac{4l}{\pi d^2 R_b} \qquad \text{(Equation 1)}$$

where σ is the ionic conductivity (Scm^{-1}), l is the thickness of polymer film sample (cm), A represents the surface area of the stainless–steel blocking electrode (cm^2), R_b stands for the bulk resistance of the polymer electrolyte (Ω) and d is the electrode diameter. The thicknesses of the copolymer electrolytes were measured by micrometer screw gauge. The diameter of the blocking electrode is 2.5 cm. The R_b was determined from the intercept of low frequency spike and the real part of complex impedance (Z') at x–axis. The measurement was taken from room temperature to 80 °C.

2.3.2. Transference number study

Freshly prepared PVdF–HFP/LiClO$_4$/BmImCl solid copolymer electrolyte was polarized under a fixed DC voltage of 0.08 V. Stainless steel electrodes were used as blocking electrodes. The solid copolymer electrolytes were then sandwiched between these electrodes. The total ionic transference numbers: ionic transference number (t_{ion}) and electronic transference number ($t_{electron}$) were evaluated by using the Wagner's polarization technique.

2.3.3. X–ray diffraction (XRD)

The XRD patterns of PVdF–HFP/LiClO$_4$/BmImCl solid copolymer electrolytes were investigated by means of Siemens D 5000 diffractometer with Cu–K$_\alpha$ radiation (λ=1.54060 Å), over the range of 2θ=5–80° at ambient temperature.

### 2.3.4. Differential scanning calorimetry (DSC)

DSC was carried out by TA Instrument Universal Analyzer 200 which comprised of DSC Standard Cell FC as main unit and Universal V4.7A software. Samples weighing 5 mg hermetically sealed in the aluminum T zero pans were subjected to DSC analyzer with a reference cell which is comprised of an empty hermetically sealed aluminum pan. Six cycles were recorded in the DSC analysis. As a preliminary step, the samples were initially heated from 25 °C to 105 °C to remove any trace amount of solvent and trapped moisture at a heating rate of 10 °C min^{-1}. The heating process was maintained for 5 minutes to ensure the complete of the dehydration process. The samples were equilibrated to 25 °C and reheated to 200 °C at the same heating rate. The samples were cooled down sequentially to 0 °C at the cooling rate of –10 °C min^{-1} to remove the thermal history of the samples. It is followed up by the heating process from –50 °C to 200 °C at the same heating rate. The samples were eventually cooled down to –50 °C at the same cooling rate. The final heating and cooling processes were used to determine glass transition temperature (T_g), melting temperature (T_m) and crystallization temperature (T_c) through endothermic and exothermic reactions, respectively. The crystallinity of polymer electrolytes was further calculated. All the measurements are conducted under a nitrogen flow rate of 10 ml min^{-1}.

2.3.5. Thermogravimetric Analysis (TGA)

TGA were performed by TA Instrument Universal Analyzer 500 with Universal V4.7A software. Samples weighing 2 mg were heated from 25 °C to 580 °C at a rate of 20 °C min^{-1} under a nitrogen atmosphere.

3. RESULTS AND DISCUSSION

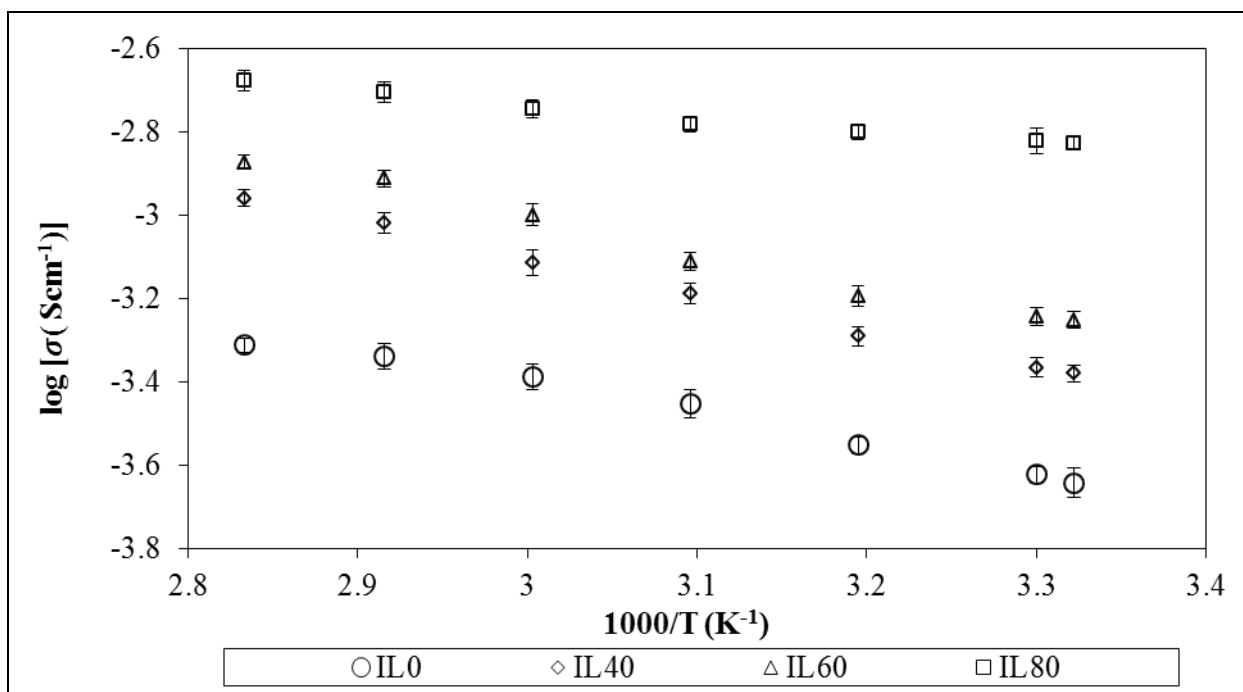*3.1. Ambient temperature–ionic conductivity studies*
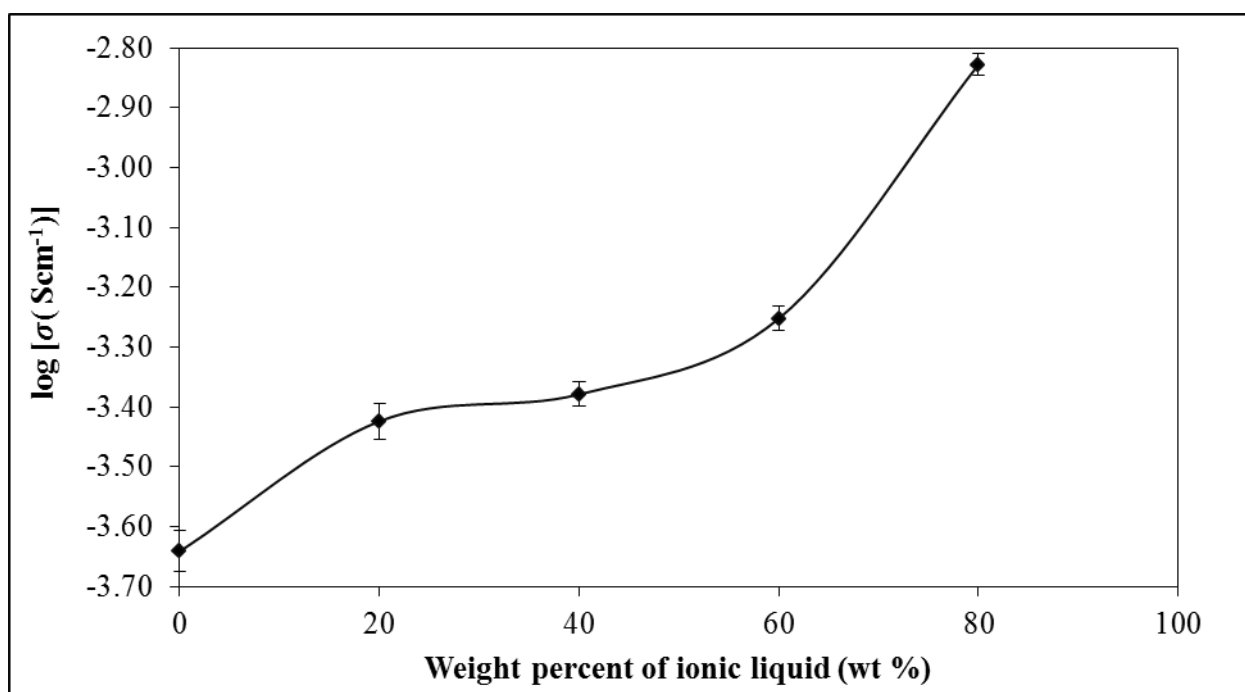
Figure 1. Logarithm of ionic conductivity of polymer electrolytes with respect to the weight ratio of ionic liquid at ambient temperature.

Figure 1 portrays the logarithm of ionic conductivity versus weight ratio of ionic liquid incorporated into PVdF–HFP/LiClO$_4$ at room temperature. The ionic conductivity is slightly increased from IL0 $(2.28\pm0.03)\times10^{-4}$ Scm^{-1} to $(3.77\pm0.03)\times10^{-4}$ Scm^{-1} by adding 20 wt% of ionic liquid into the polymer system. The ionic conductivity is further increased to the maximum level of $(1.49\pm0.02)\times10^{-3}$ Scm^{-1} upon adulteration of 80 wt% of ionic liquid.

3.2. Temperature–dependent ionic conductivity studies

Figure 2 depicts the ionic conductivity of PVdF–HFP/LiClO$_4$ in the temperature regime, from ambient temperature to 80 °C with respect to the concentration of BmImCl. All the plots show the linear relationship where their regression value approaches to zero.

Figure 2. Temperature dependence–ionic conductivity of PVdF–HFP/LiClO₄ with respect to different weight percentage of BmImCl from room temperature to 80°C.

3.3. Transference number study
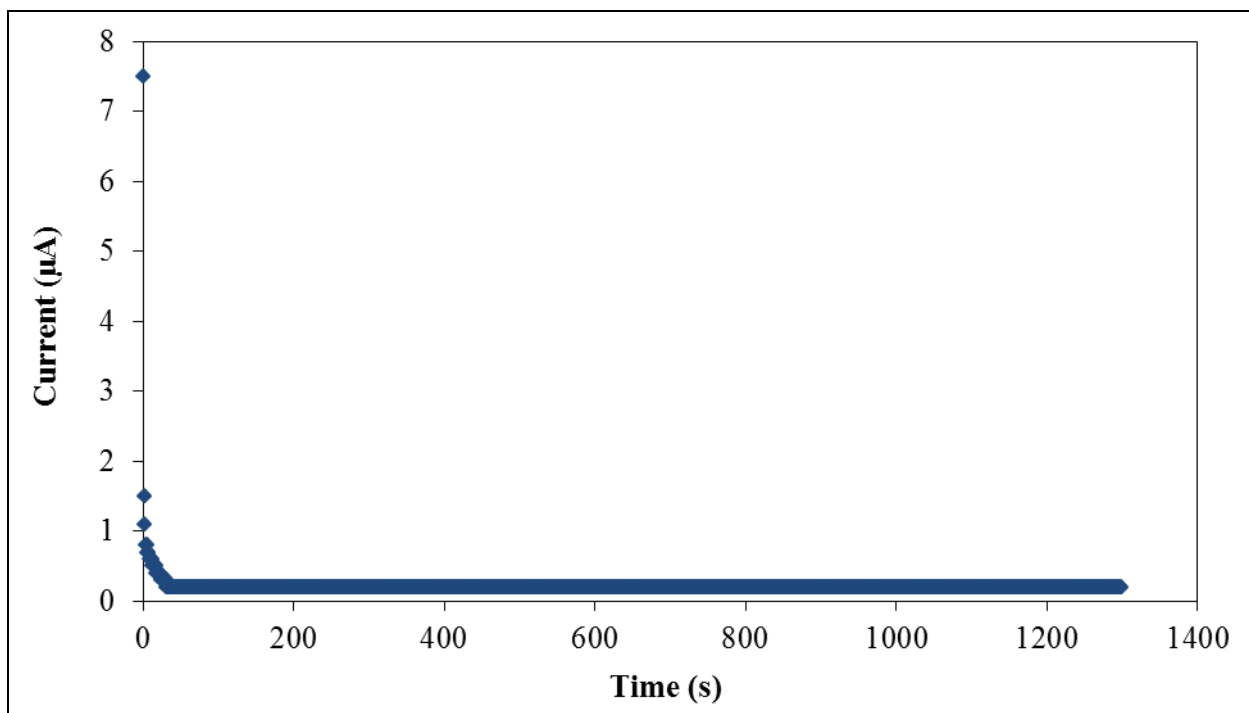
**Figure 3.** Chronoamperometry of IL80 under a 0.8 V of DC bias at room temperature.

Figure 3 visualizes the chronoamperometric curve of IL80 in the configuration of stainless steel (SS)/IL80/stainless steel (SS) under a 0.8 V of DC bias. As envisaged in the figure, the values of I_s

and I_T are 0.2 µA and 7.5 µA, respectively. Based on the calculation, the t_{ion} of 0.97 and $t_{electron}$ of 0.03 have been determined.

3.4. X–ray diffraction (XRD)
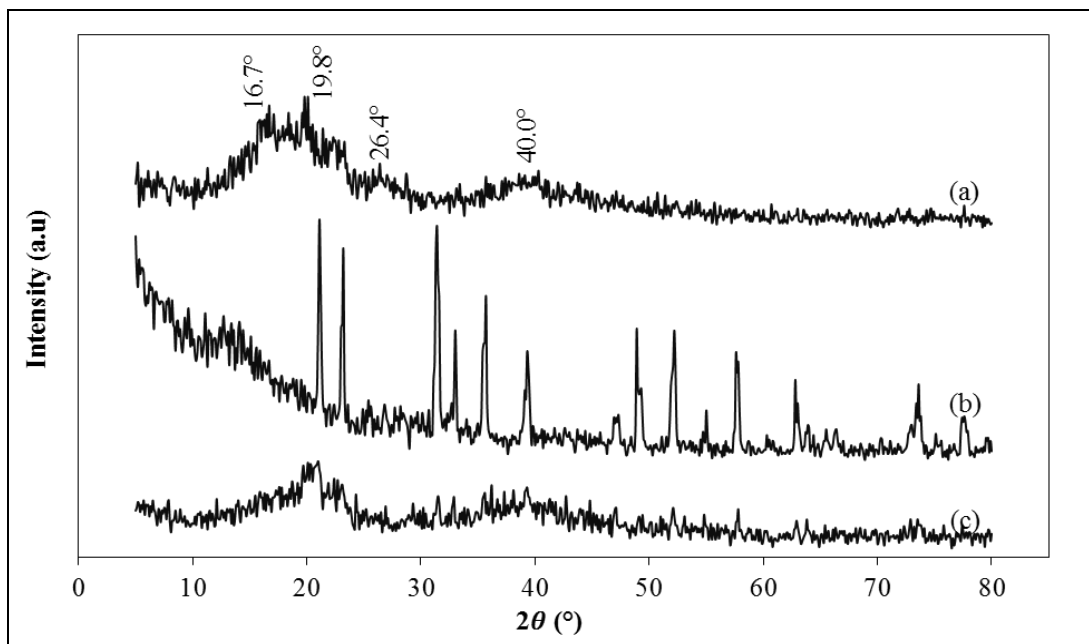
**Figure 4.** XRD diffractograms of (a) pure PVdF–HFP, (b) LiClO$_4$ and (c) IL0.
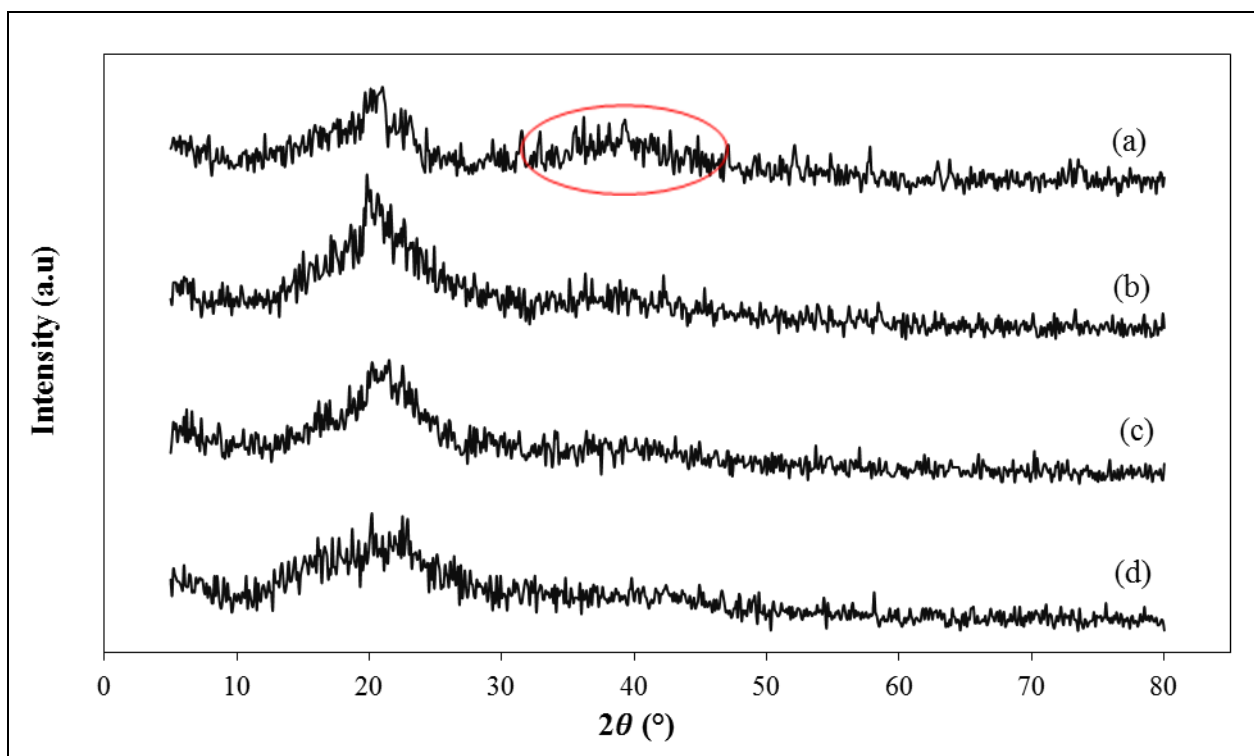
Figure 5. XRD diffractograms of (a) IL0, (b) IL40, (c) IL60 and (d) IL80.

Figure 4 shows the XRD patterns of pure PVdF–HFP, pure LiClO$_4$ and IL0. Two intense peaks are located at 2θ=16.7° and 19.8°, meanwhile two humps are obtained at 2θ=26.4° and 40° revealing the semi–crystalline behavior of polymer matrix. Moreover, the sharp diffraction peaks at 2θ=21.1°, 23.2°, 31.4°, 32.9°, 35.7°, 39.3°, 47.3°, 48.9°, 52.2°, 54.9°, 57.6°, 62.8°, 73.6° and 77.6° reveal the crystalline properties of pure LiClO$_4$. Comparing figure 4(a) with 4(c), the characteristic peaks at 2θ=16.7° and 26.4° are absent with addition of LiClO$_4$. On the contrary, the peaks at the 2θ angles of 19.8° and 40.0° manifest upward and downward shifts to 20.1° and 39.3°, respectively. On the other hand, the XRD patterns of IL0 and ionic liquid–based polymer electrolytes are illustrated in Figures 5(a)–(d). The broad characteristic peak at 2θ=39.3° is disappeared upon addition of BmImCl. On the other hand, the peak at 2θ=20.1° is shifted to 19.8°, 20.7° and 21.2° for IL40, IL60 and IL80, respectively.
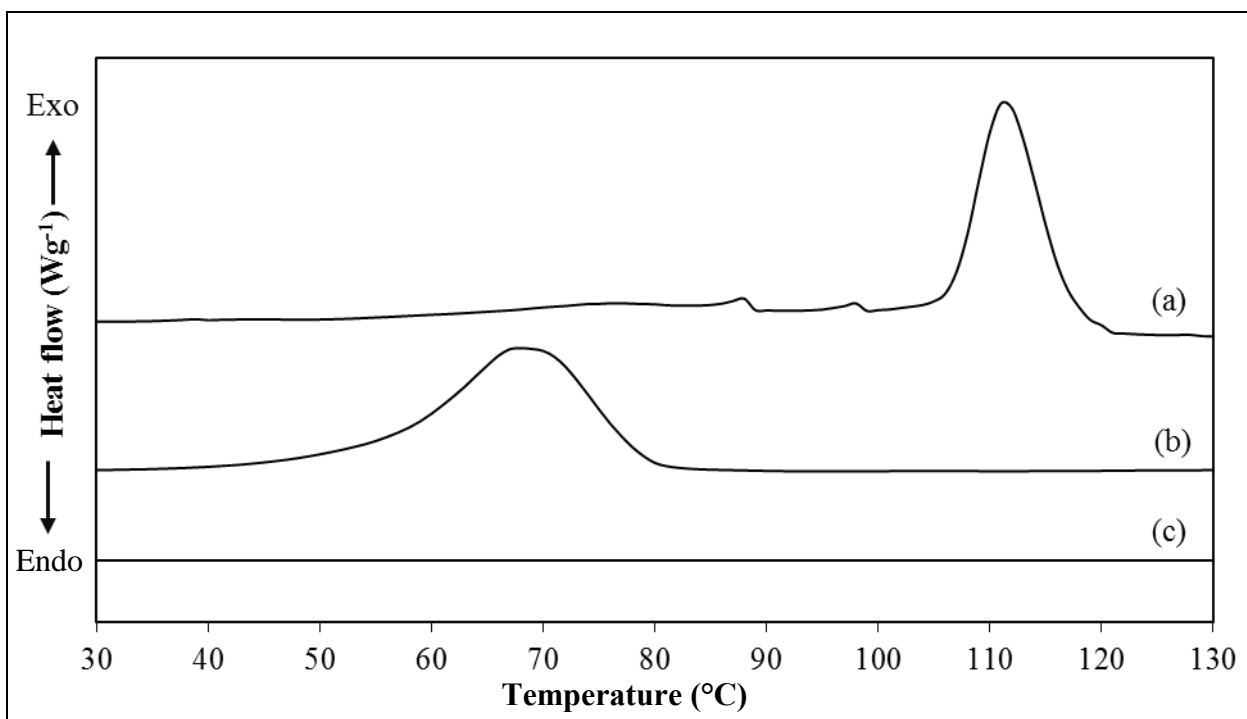
3.5. Differential scanning calorimetry (DSC)

Table 2. Glass transition temperature (T_g), melting temperature (T_m), crystallization temperature (T_c), heat of fusion (ΔH_m) and percentage of crystallinity (χ_c) of IL0, IL40 and IL80.

Sample	Glass transition temperature, T_g (°C)	Melting temperature, T_m (°C)	Crystallization temperature, T_c (°C)	Heat of fusion, ΔH_m (Jg^{-1})	Crystallinity, χ_c (%)
IL0	105.38	147.33	117.12	13.78	13.16
IL40	-21.43	119.26	69.25	9.64	9.21
IL80	-26.64	----------------------------Not detected----------------------------			
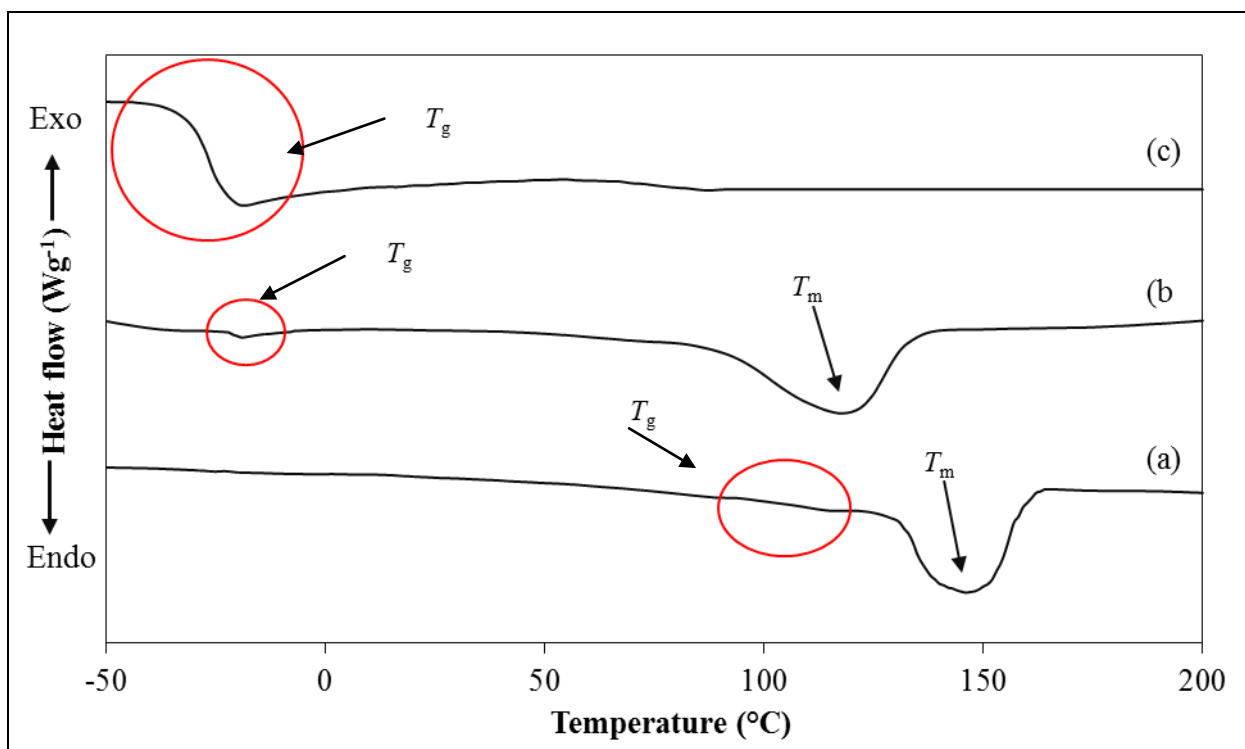
Figure 6. DSC thermograms of (a) IL0, (b) IL40 and (c) IL80 in the heating cycle.

Figure 7. DSC thermograms of (a) IL0, (b) IL40 and (c) IL80 in the cooling cycle.

Figures 6 and 7 demonstrate the DSC analyses for IL0, IL40 and IL80 in heating and cooling processes, respectively. The glass transition temperature (T_g), melting temperature (T_m), crystallization temperature (T_c), heat of fusion (ΔH_m) and percentage of crystallinity (χ_c) of IL0, IL40 and IL80 are summarized in Table 2.

The T_g of 105 °C is detected for PVdF–HFP doped LiClO$_4$. Nevertheless, upon addition of BmImCl, sub–ambient glass transition temperatures of –21 °C and –27 °C are observed for IL40 and IL80, respectively. The T_m of IL0 is 147 °C. Upon addition of 40 wt% of BmImCl, the peak position has been shifted to 119 °C. In contrast, the melting point of IL80 is absent. The crystallinity of 13.16% and 9.21% has been further determined for IL40 and IL80, respectively. A sharp exothermic crystallization peak is attained at 117 °C for IL0. This crystallization temperature is shifted towards lower temperature that is 69 °C when 40wt% of BmImCl is embedded into polymer complex. Again, the crystallization temperature is not appeared upon addition of 80 wt% of BmImCl. Based on Table 2, the heat of fusion and degree of crystallinity are reduced by embedding ionic liquid into the polymer complexes.

3.6. Thermogravimetric Analysis (TGA)

Figure 8 illustrates the thermogravimetric analysis of pure PVdF–HFP, IL0 and IL40. There is only one degradation step in pure PVdF–HFP as shown in Figure 8. However, four and two decomposition curves have been observed for IL0 and IL80, respectively.
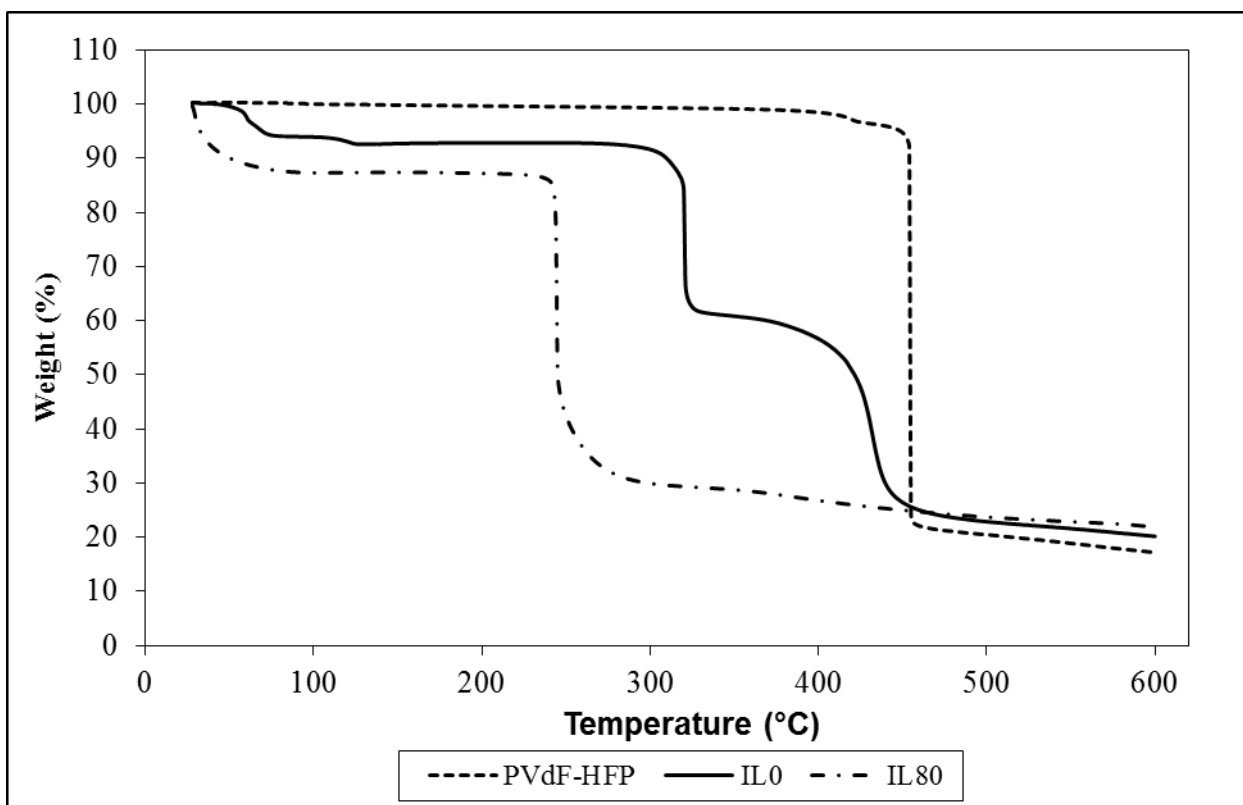
Figure 8. Thermogravimetric curves for pure PVdF–HFP, IL0 and IL80.

4. DISCUSSION

4.1. Ambient temperature–ionic conductivity studies

The ionic conductivity increases with the mass loadings of BmImCl. The ionic conductivity of IL80 is increased by one order of magnitude compared to IL0. The major contributor is the strong plasticizing effect of ionic liquid. The ionic liquid would act as plasticizer to soften the polymer backbone and enhance the flexibility of polymer matrix. The lithium charge carriers could be decoupled more easily with highly flexible polymer matrix. In addition, the flexible polymer backbone could speed up the polymer segmental mobility. As a result, this promotes the ionic hopping mechanism within the polymer electrolytes which in accordance with higher ionic conductivity [17]. Adulteration of ionic liquid could reduce the glass transition temperature (T_g) of polymer matrix. It defined as an inherent temperature that changes the amorphous portion of polymer matrix from glassy state to rubbery state. The polymer matrix is hard and stiff at a glassy state. So, the mobility of polymer segments is restricted below T_g. However, above T_g, the glassy state is converted into rubbery state which is soft and elastomeric. The polymer backbone is accompanied by more long range molecular motion (i.e. segmental motion) at this stage. Therefore, the bond rotation of the polymer chain and kinetic energy of the molecules are increased. Higher degree of rotation freedom of molecules within the polymer backbone promotes the decoupling of the charge carriers (or denoted as

lithium cations in this study) and hence favors the ionic transportation which leads to increase in ionic conductivity.

Besides, ionic liquid would weaken the transient coordinative bonds between charge carriers and electron withdrawing group (fluoride anions) of polymer backbone. Hence, more lithium cations (Li^+) would be dissociated from the coordination bond by doping ionic liquid. This induces to higher ionic conductivity and ultimately kicks off the ion migration in the polymer electrolyte, initiating the ionic conduction process [18]. We suggest that the inclusion of ionic liquid might destroy the ordered arrangement of crystalline structure of polymer chain and improve the amorphous degree of the polymer matrix. Higher amorphous proportion of polymer electrolytes could provide highly flexible polymer backbone and thus promote the mobility of polymer segments within the polymer electrolytes. As a result, it endorses the dissociation of charge carriers from the interactive bonds and favors the ionic transportation, increasing the ionic conductivity. Therefore, it can be concluded that the ionic liquid can enhance the ionic conductivity of polymer electrolytes through three ways: softening the polymer backbone, weakening the transient coordination bonds and demolishing the ordered structure of crystalline portion. Since IL 80 achieves the highest ionic conductivity at ambient temperature, thus the segmental mobility and amount of mobile charge carriers of IL80 are in the optimum level. However, beyond this mass fraction, the polymer electrolyte becomes mechanically unstable. So, the ionic conductivity could not be determined for the continuous sample.

4.2. Temperature–dependent ionic conductivity studies

The temperature dependence–ionic conductivity study displays a linear relationship for all polymer electrolytes suggesting an Arrhenius–type thermal activated process as the regression values approach to unity. This theory reveals the ionic hopping mechanism in the polymer electrolytes. Ion hopping mechanism happens between coordinating sites and local structural relaxations [19]. As explained in section 4.1, it implies that the ionic liquid would break the interactive bonds between the Li^+ and fluoride anions (F^-) from polymer matrix. Thus, Li^+ is detached from the polymer backbone. An empty site has been created after the Li^+ decoupling process. Consequently, the Li^+ from adjacent sites would occupy this vacant space and hence reform the coordination bond with the polymer. The ionic hopping mechanism is eventually generated.

As can be seen, the ionic conductivity increases with temperature. The movement of ions in the solid polymer electrolyte is aided by the great amplitude of polymer segmental motion at higher temperature. Therefore, as the temperature increases, the polymer chain produces faster internal bond rotation which rises up the segmental mobility. The segmental motion facilitates the intra– and inter–ionic hopping in the polymer chain, and hence provides a route for ion transportation [20]. Apart from that, the vibrational mode of Li^+ is higher upon heating. This results a weaker coordination bond between polymer and lithium cation and promotes the ion dissociation. Thus, the migration of ions within polymer complexes could be easier which contributes to higher ionic conductivity at higher temperature [21].

4.3. Transference number study

Transference number analysis is employed to determine ionic or electronic conduction in the polymer electrolytes by using Wagner's polarization technique. Ionic transference number (t_{ion}) and electronic transference number ($t_{electron}$) can be determined by using formula below:

$$t_{ion} = 1 - \frac{I_s}{I_T} \qquad \text{(Equation 2)}$$

$$t_{electron} = \frac{I_S}{I_T} \qquad \text{(Equation 3)}$$

where I_S and I_T are denoted as steady–state current and total current, respectively. In this principle, I_T is the initial current consisting of both ionic and electronic current at t=0, meanwhile I_S is comprised of electronic current where the current has reached the steady state. As can be seen, the ionic transport number is far outweighed than the electronic transference number. Consequently, this concluded that the ion conduction domain in the polymer matrix as the electron conduction is negligible [18].

4.4. X–ray diffraction (XRD)

XRD reveals the structural change with addition of LiClO$_4$ and BmImCl. Four characteristic peak at 2θ=18.2°, 20°, 26.8° and 38° which correspond to the (1 0 0), (0 2 0), (1 1 0) and (0 2 1) crystalline planes of PVdF are reported in literature [22]. Similarly, four diffraction peaks also found for pure PVdF–HFP, as shown in Figure 4(a). All these characteristic peaks pertaining to LiClO$_4$ are disappeared in Figure 4(c). This entails the well dissolution of LiClO$_4$ into the PVdF–HFP polymer system. The disappearance of 2θ=16.7° and 26.4° indicates that the crystalline planes of (1 0 0) and (0 2 1) are no longer appeared due to the complexation between PVdF–HFP and LiClO$_4$. This also proves the enhancement of amorphousness of the polymer electrolytes upon inclusion of LiClO$_4$. Furthermore, the peaks at the 2θ angles of 19.8° and 40.0° have been shifted to 20.1° and 39.3°, respectively. These shifting signify the complexation between PVdF–HFP and LiClO$_4$. Apart from shifting, they undergo the changes in intensity. The intensities of the peak and hump are significantly decreased by adding LiClO$_4$ into PVdF–HFP polymer matrix. This reflects that the crystallinity of polymer electrolytes has been considerably diminished which helps in improving the ionic conductivity.

An obvious observation is perceived upon addition of BmImCl. A broad characteristic peak is present at 2θ=39.3° for IL0 as highlighted in Figure 5(a). However, this peak is completely vanished with doping of BmImCl. More amorphous phase of polymer system is disclosed with the absence of this crystalline peak. In addition, the peak shifting is obtained for the characteristic peak at 2θ=20.1° with inclusion of BmImCl. This divulges that the incorporation of ionic liquid changes the crystallographic organization of polymer electrolytes. Apart from the peak shifting, this peak becomes broader upon insertion of ionic liquid. The width of this peak boosts with the ionic liquid mass loadings. The relative peak intensity is also significantly reduced. All these phenomena propose that ionic liquid disrupts the disordered arrangement of polymer matrix and thereby reduces the crystalline

region [18]. In other word, doping of ionic liquid amplifies the amorphous proportion of polymer complex. Higher amorphous proportion of polymer electrolytes could provide more flexible polymer backbone as explained in section 4.1. Thus it enhances the segmental mobility and promotes the ion decoupling from coordinative bonds, resulting in higher ionic conductivity.

4.5. Differential scanning calorimetry (DSC)

A small drop in heat flow is firstly attained in DSC thermogram when the sample is heated. It is well known as glass transition temperature (T_g). The ionic liquid reduces the glass transition temperature which induces to higher segmental motion of polymer chain as discussed in section 4.1. This can be proven in this study. As can be seen, the T_g is greatly reduced by adding BmImCl. The lower in T_g implies the ease of phase transition from glassy state to rubbery state. Thus, it facilitates the ionic hopping above this temperature which in accordance with higher ionic conductivity as explained in section 4.1. The drop in heat flow of IL80 is relatively higher than IL40 and IL0. This divulges higher amorphous phase of IL80.

The T_g is then followed up by a sharp endothermic peak which denoted as melting point of polymer electrolyte (T_m). As reported in Ramesh and Lu (2011), pure PVdF–HFP shows T_m at 140 °C. However, T_m has been increased by 7 °C with addition of LiClO$_4$ due to the complexation between polymer and salt. These transient coordinative bonds require higher energy to exhibit the phase transition from solid state to liquid state. However, the T_m is shifted to lower temperature with addition of 40 wt% of BmImCl. The downward shift in T_m is a result of reduction in crystallinity or localized influence on the polymer chain conformation [23]. It is reminiscent of disturbance of ordered arrangement of polymer chain. Therefore, the entanglements and those interactive bonds within the polymer matrix can be demolished easily. Hence, lesser energy is required to break the bonds. The result is in good agreement with XRD findings. Moreover, the ionic liquid could weaken the interactive bonds in the polymer complex. As a result, the total amount heat used to break the coordination bonds is lesser. No melting point is detected with increasing the ionic liquid content further. The disappearance of melting point for IL80 indicates a complete structural change of polymer electrolyte from semi–crystalline region to amorphous phase. The structural alteration credits to BmImCl which stop the crystallization process [24].

For cooling scan, a sharp exothermic peak is attained in Figure 7. This peak is assigned as crystallization temperature (T_c). Above T_g, the polymer molecules start to gain the freedom in motion. The macromolecules will arrange themselves spontaneously into a crystalline form when they have enough freedom of motion. Thus, the crystallization is occured at this state and the temperature for the crystallization is defined as T_c. As the polymer is further heated, it will lose its elastometric properties and hence melt to a flowable liquid. At this point, the crystalline melting temperature, T_m is reached. So, the T_c is normally occurred at lower temperature in comparison to T_m. The crystallization temperature of 117 °C and 69 °C are observed for IL0 and IL40, as shown in Figures 7(a) and (b). The crystallization temperature is reduced upon addition of 40 wt% of BmImCl. It is attributed to the lower in crystalline portion of polymer matrix with addition of BmImCl as ionic liquid could disrupt the

ordered arrangement of polymer structure easily. Therefore, the crystallization occurs at lower temperature than IL0. However, no T_c is attained with adulteration of 80 wt% of BmImCl. This confirms again the structural changes from semi–crystalline to amorphous region in IL80.

The ionic liquids could disrupt the ordered arrangement of polymer electrolytes, as suggested in section 4.1. This can be proven through the crystallinity determination. In order to verify the amorphousness of polymer electrolytes, the crystallinity of polymer electrolytes has been calculated. The equation below is employed to determine the crystallinity of a polymer:

$$\chi_c = \left(\frac{\Delta H_m}{\Delta H_m^{\theta}} \right) \times 100\% \qquad\qquad\qquad \text{(Equation 4)}$$

where χ_c is percentage crysallinity, ΔH_m represents the heat of fusion of sample at the melting point and ΔH_m^{θ} denotes the reference heat of the fusion of the crystalline α–PVdF, 104.7 Jg^{-1} at the equilibrium melting temperature [11]. This formula normalizes the heat of fusion of a sample to that of a 100% crystalline sample of the same polymer. ΔH_m of the sample is the area under the curve of melting peak which can be computed by software TA Universal Analysis software. Besides peak shifting, the area under the curve of the endothermic peak of IL40 is smaller compared to IL0. Thus, the degree of crystallinity is also reduced when 40 wt% of BmImCl is added into the polymer electrolyte. The result is commensurate with the XRD study. The heat of fusion and degree of crystallinity of IL80 are not determined as the crystalline melting peak is absent. The decreased in crystallinity verifies that ionic liquid helps in disrupting the ordered arrangement of polymer matrix and hence decreases the crystalline phase which imparts to higher amorphous region. The theory is also applied onto the smaller heat of fusion of IL40. The crystalline region is vaguely reduced by adding 40 wt% of BmImCl. Therefore, lesser energy is required to melt the crystallite as the amount of crystallite within IL40 is lesser.

4.6. Thermogravimetric Analysis (TGA)

Thermogravimetric analysis (TGA) is conducted to investigate the thermal stability of polymer membrane. Figure 8 illustrates the thermogravimetric analysis of pure PVdF–HFP, IL0 and IL40. No solvent is observed in this degradation curve for pristine PVdF–HFP. It proves that acetone is completely evaporated [15]. Only a weight loss of 80% is observed for pure PVdF–HFP as exemplified in figure 8. As can be seen, PVdF–HFP starts to be decomposed at 402 °C with a residual mass of around 20%. The unzipping process is favorable at high temperature which induces to some degradation processes such as random chain scission reaction, depolymerization, inter–molecular transfer reaction and intra–molecular transfer reaction. At the end, the monomer and oligomers which chemi–absorbed onto polymer matrix would be decomposed in this temperature regime [18].

However, four stages of weight loss have been observed for IL0. A small weight loss of 5% is attained at around 65 °C due to acetone evaporation. The following weight loss of 3% corresponds to dehydration of water as polymer and salt are hygroscopic compounds. A stable weight has been maintained until 294 °C. The third mass loss of 31% is interpreted thereafter. The main contribution of this weight loss comes from loss of dopant percholate (ClO_4) anions which bound to PVdF–HFP.

According to Sari et al., the presence of polymer will reduce the decomposition temperature of ClO_4 anions. This can be proven in this study. IL0 starts to be degraded at 294 °C and it is lower than pure $LiClO_4$ where its decomposition temperature is 420–540 °C [25]. The last weight loss of 42% happens from 325 °C to 600 °C with residual mass of 21% and it corresponds to the degradation of polymer matrix. As explained above, the disintegration could cause a decrease in molecular weight of polymer chain and ultimately lead to mass loss at high temperature. The starting degradation temperature of pristine PVdF–HFP is around 400 °C, whereas the temperature is remarkably reduced by adding $LiClO_4$. So, it leads to a conclusion that the introduction of $LiClO_4$ into the polymer system decreases the stability of the polymer composition drastically. The thermal destruction is mainly due to the catalytic effect of this salt [26].

However, based on the TGA curves, only two stages have been observed for IL80 upon heating. IL80 has a drastic weight loss of 12% in the initial stage. The vaporizations of remaining solvent, moisture and impurities are the attributors [27]. It is followed up by a weight loss of 64% at 232 °C with a residual mass of 23%. This significant decrease in weight is primarily due to the decomposition of polymer chain, as explained above. The thermal properties of ionic liquid–based polymer electrolyte is better than $LiClO_4$–doped based polymer electrolyte and pure PVdF–HFP as it manifests higher residual mass after a prolonged heating process. The thermal stability of IL80 is up to 232 °C. However, it is lower than other polymer systems in comparison to pure PVdF–HFP and IL0 because of the growth of amorphous fraction [28]. Nevertheless, it is still a promising candidate for battery application where its operating temperature is normally in the range of 30–80 °C.

5. CONCLUSION

The goal of this research is to investigate effect of ionic liquid, BmImCl on PVdF–HFP solid copolymer electrolytes with incorporation of $LiClO_4$ via solution casting method. The properties of PVdF–HFP/$LiClO_4$ with different weight ratio of BmImCl were characterized. The highest conductivity of $(1.49\pm0.02)\times10^{-3}$ Scm^{-1} was achieved with doping of 80 wt% of BmImCl at room temperature. Addition of BmImCl had enhanced the ionic conductivity by decreasing the crystallinity and glass transition temperature of polymer matrices. These copolymer electrolytes obeyed the Arrhenius theory in the temperature dependent–ionic conductivity study. The ionic hopping mechanism is further revealed. Addition of ionic liquid reduced the crystalline phase of polymer complex as shown in XRD diffractograms. The reduction of glass transition temperature is also proven in DSC findings. The melting and crystallization temperatures of copolymer electrolyte containing 80 wt% of BmImCl are absent. This deduced the phase transformation from semi crystalline to amorphous. The degree of crystallinity of these copolymer electrolytes were further determined in order to prove the amorphousness of polymer matrix. The thermal stability of solid polymer electrolyte was declined with addition of ionic liquid. However, the copolymer electrolytes containing 80 wt% of BmImCl starts to be decomposed at 232 °C which is suitable for most application.

References

1. J. Reiter, O. Krejza, M. Sedlaříková, *Sol. Energy Mater. Sol. Cells* 93 (2009) 249–255.
2. Ramesh, C.–W. Liew, *J. Non–Cryst. Solids* 358 (2012) 931–940.
3. M.Aparicio, J. Mosa, M. Etienne, A. Durán, *J. Power Sources* 145 (2005) 231–236.
4. J. Y. Song, Y. Y. Wang, C. C. Wan, *J. Power Sources* 77 (1999) 183–197.
5. Y. J. Hwang, K. S. Nahm, T. P. Kumar, A. M. Stephan, *J. Membr. Sci*. 310 (2008) 349–355.
6. A. L. Saroj, R. K. Singh, *J. Phys. Chem. Solids* 73 (2012) 162–168.
7. E. Kowsari, Advanced Applications of Ionic Liquids in Polymer Science in Ionic Liquids: Applications and Perspectives, In Tech, Croatia, 2011, pp. 1–28.
8. V. Aravindan, P. Vickraman, *Eur. Polym. J*. 43 (2007) 5121–5127.
9. R. Miao, B. Liu, Z. Zhu, Y. Liu, J. Li, X. Wang, Q. Li, *J. Power Sources* 184 (2008) 420–426.
10. A. M. Stephan, S. G. Kumar, N.G. Renganathan, M. A. Kulandainathan, *Eur. Polym. J*. 41 (2005) 15–21.
11. S. Ramesh, S.–C. Lu, *J. Mol. Struct*. 994 (2011) 403–409.
12. C.–G. Wu, M.–I. Lu, H.–J. Chuang, *Polym.* 46 (2005) 5929–5938.
13. S. Wang, S. Jeung, K. Min, *Polym.* 51 (2010) 2864–2871.
14. Xu, Kang. *Chem. Rev*. 104 (2004) 4303–4417.
15. K.S. Kim, S.Y. Park, S. Choi, & H. Lee, *J. Power Sources* 155 (2006) 385–390.
16. S. S. Sekhon, P. Krishnan, B. Singh, K. Yamada, C.S. Kim, *Electrochim. Acta* 52 (2006)1639–1644.
17. C.–W. Liew, S. Ramesh, K. Ramesh, and A. K. Arof, *J. Solid State Electrochem*. 16 (2012)1869–1875.
18. S. Ramesh, C.–W. Liew, K. Ramesh, *J. Non–Cryst. Solids* 357 (2011) 2132–2138.
19. D. F. Vieira, C. O. Avellaneda, A. Pawlicka, *Electrochim. Acta* 53 (2007) 1404–1408.
20. Y. F. Wang, X. Y. Ma, Q. L. Zhang, N. Tian, *J. Membr. Sci*. 349 (2010) 279–286.
21. G. G. Kumar, P. Kim, A.R. Kim, K. S. Nahm, R. N. Elizabeth, *Mater. Chem. Phys*. 115 (2009) 40–46.
22. G. G. Kumar, P. Kim, A. R. Kim, K. S. Nahm, R. N. Elizabeth, *J. Membr. Sci*. 303 (2007) 126–131.
23. K. S. Kim, S. B. Lee, H. J. Lee, H. S. Kim, Y. W. Lee, K. S. Kwack, *J. Ind. Eng. Chem*. 15 (2009) 657–660.
24. L. Wang, N. Li, X. M. He, C. R. Wan, Y. I. Chang, *Electrochim. Acta* 68 (2012)214–219.
25. J.–H. Hong, L. Song, X.–W. Zhou, K. Diakite, K.–L. Zhang. *Chem. Res. Chin. Univ*. 26 (2010) 300–303
26. E. M. Shembel, O.V. Chervakov, L. I. Neduzhko, I. M. Maksyuta, Y. V. Polischyk, D. E. Reisner, P. Novak, D. Meshri, *J. Power Sources* 96 (2001) 20–28.
27. S. Rajendran, O. Mahendran, T. Mahalingam, *Eur. Polym. J*. 38 (2002) 49–55.
28. Y. J. Shen, P. P. Chu, Solid State Ionics: Trends in the New Millennium, World Scientific Publishing, Singapore, 2002, pp.361–368.